MECHANICS OF COHESIVE-FRICTIONAL MATERIALS, VOL. 1, 95–114 (1996)

A multiphase medium model for localisation and postlocalisation simulation in geomaterials

B. A. Schrefler, L. Sanavia and C. E. Majorana

Istituto di Scienza e Tecnica delle Costruzioni, Università di Padova, via Marzolo 9, 35131, Padova, Italy

SUMMARY

It is recalled that negative water pressures are of importance in localisation phenomena of fully saturated, undrained samples of dilatant geomaterials. A model to simulate cavitation phenomena connected with such pore water tractions is developed and implemented in a simplified form in a dynamics code for partially saturated porous media. A case of localisation is studied from the onset of the instability up to the full developed shear band. The weak mesh dependence of the maximum effective plastic strain, due to the employed physical model, is also shown.

KEY WORDS: multiphase material; strain localisation; averaging theories; pore pressure; cavitation; finite element method

1. INTRODUCTION

Dilatant geomaterials, i.e. fissured rocks, dense sands, stiff clays, increase the porosity when subjected to sufficiently high deviatoric stresses. If these materials are saturated with a pore fluid and the pore volume increases more rapidly than the fluid can flow into it, the pore pressure decreases. This means an increase in effective compressive stress which inhibits further inelastic deformation up to a certain limit. The phenomenon is called dilatant hardening or strengthening and was first discussed by Reynolds in 1885 in his studies on granular materials[1].

Rice[2] investigated with a mathematical model the amount of dilatant strengthening in a fully saturated dilatant frictional material. This analysis demonstrates that '... dilatant hardening is stable only in those circumstances for which the underlying drained deformation would be stable: $H > 0$.' H is the plastic hardening modulus. Rudnicki[3] analysed then a fluid saturated rock mass with an embedded weakened layer and came to similar conclusions: '... solutions to the linearized equations become unstable ... when conditions for localisation of deformation are met in terms of the drained response of the embedded layer, but final instability does not occur until these conditions are met in terms of the undrained response of the embedded layer.' Vardoulakis[4] adds to the mathematical model an inertia term and shows the importance of dynamic stability analysis in case of undrained simple-shear deformation of water-saturated granular soil, at least when the material is contractant. He comes to the conclusion that: 'Contractant material becomes unstable (liquefies) at the state of maximum shear, whereas dilatant material becomes unstable after the state of maximum stress obliquity is reached in the softening regime of the background drained behaviour.'

Loret and Prevost[5] studied with a numerical model shear band dominated processes in a large fully saturated soil mass using dynamic strain localisation theory. A high frequency situation was

CCC 1082–5010/96/010095–20

Received 27 September 1995
Revised 14 November 1995

investigated, where a velocity jump was applied at the boundary of the specimen. They pointed out correctly that the presence of pore fluid may delay shear band formation.

The importance of pore pressure in localisation phenomena was however not appreciated to a full extent: in none of the above papers[2–5] the possibility of negative pore pressure, i.e. pore water tractions, are mentioned. Such pore water tractions were however observed experimentally by Mokni[6] in undrained samples of dense sand. Starting with different backpressures, strain localisation did only start when pore water tractions of the order of 80 kPa developed.

Similar negative pore pressures have been obtained independently by us with a numerical model[7] based on dynamic shear band localisation, applied to a large soil mass as in Reference 5. In our case we used ramp loading (low frequency situation). At the negative pressures where localisation takes place, pore water cavitates, i.e. boils at ambient temperature and a second fluid phase is present. Hence a numerical model should include the capability to model this phenomenon.

We show here a full model for thermohydromechanical analysis of partially saturated porous media capable of simulating phase change phenomena connected with cavitation. A numerical solution exists for this model,[8] but at the moment only in the case of slow phenomena, without inertia effects.

Since inertia effects are important, certainly for contractant material[4] but also for dilatant material, given the speed at which the shear band develops after its onset,[7] we show a simplified dynamic model which incorporates some of the features of the full model. This model is a development of the code Swandyne[9,10] which simulates dynamic partially saturated soil behaviour with gas (air) phase at constant (atmospheric) pressure.

The multiphase material approach adopted in our model has a further advantage.[7] In the mass balance equations appears a Laplacian, which is known to regularise the solution. The obtained maximum effective plastic strain is reasonably well mesh independent as shown by numerical experiments. This means that a regularisation is contained in the physics of the problem. Two examples will show this and the other above mentioned features of our model.

2. Mathematical model

2.1. Physical model, thermodynamic relations and constitutive equations

The full thermohydromechanical model necessary to simulate phase change in fully and partially saturated porous media was developed[11] using averaging theories following Hassanizadeh and Gray.[12–14] The underlying physical model and the most important equations are briefly summarized in what follows.

The partially saturated porous medium is treated as multiphase system where the voids of the skeleton are filled partly with liquid and partly with gas assumed to behave as an ideal mixture of dry air and water vapour. The state of the medium is described by water pressure p^w, capillary pressure p^c, temperature T and displacement vector of the solid matrix $\mathbf{u}$. Small displacements are assumed for the development of the equations. Thermal equilibrium between solid matrix, gas and liquid phases is assumed, so the temperature is the same for the three constituents.

The saturation of liquid water S_w is an experimentally determined function of capillary pressure p^c and temperature T:

$$S_w = S_w(p^c, T), \tag{2.1}$$

while its pressure p^w can be expressed at equilibrium state[15] as

$$p^w = p^g - p^c, \tag{2.2}$$

where p^g is the moist air (gas) pressure (mixture of dry air and vapour).

The equation of state of perfect gases and Dalton's law, applied to dry air (ga), vapour (gw) and moist air (g) give

$$p^{ga} = \rho^{ga} RT/M_a, \qquad p^g = p^{ga} + p^{gw}, \tag{2.3}$$

$$p^{gw} = \rho^{gw} RT/M_w, \qquad \rho^g = \rho^{ga} + \rho^{gw}, \tag{2.4}$$

Due to the curvature of the meniscus separating the liquid (water) phase from the gas phase inside the pores of the medium (considered as a capillary porous body), the equilibrium vapour pressure can be obtained from the Kelvin relationship which gives the relative humidity (RH) of the moist air inside the pores

$$RH = \frac{p^{gw}}{p^{gws}} = \exp\left(-\frac{p^c M_w}{\rho^w RT}\right), \tag{2.5}$$

where the water vapour saturation pressure p^{gws}, which depends only upon temperature T, can be obtained from the Clausius–Clapeyron equation or from empirical correlations, see, for example, Reference 16. The constitutive law for the solid phase is introduced through the concept of modified effective stress σ' (Bishop stress)

$$\boldsymbol{\sigma}' = \boldsymbol{\sigma} + p\mathbf{I}, \tag{2.6}$$

where $\boldsymbol{\sigma}$ is the total Cauchy stress tensor, $\mathbf{I}$ is the unit second-order tensor and p is an average pressure of the mixture of fluids surrounding the grains, which in the case of small dependence of Helmholtz free energies on void fraction is given[15] by the commonly employed relation

$$p = S_w p^w + (1 - S_w) p^g - p_{atm}. \tag{2.7}$$

The last term in (2.7) has been added because we use here absolute pressures; pure atmospheric pressure does not cause deformation of the medium.

The constitutive relationship for the solid skeleton has the form

$$\mathrm{d}\boldsymbol{\sigma}' = \mathbf{C}_T(\mathrm{d}\boldsymbol{\varepsilon} - \mathrm{d}\boldsymbol{\varepsilon}^T - \mathrm{d}\boldsymbol{\varepsilon}^0), \tag{2.8}$$

where $\mathbf{C}_T$ is a tangent constitutive tensor, $\mathrm{d}\boldsymbol{\varepsilon}^T = \mathbf{I}\beta_s \mathrm{d}T$ is the strain increment caused by thermoelastic expansion, β_s means the cubic thermal expansion coefficient of the solid and $\mathrm{d}\varepsilon^\circ$ represents the autogeneous strain increments and the irreversible part of the thermal strains tensor.[17]

For a binary gas mixture (dry air and water vapour), Fick's law gives the following relative average velocities $\mathbf{v}_\pi^d$ of the diffusing species

$$\mathbf{v}_{ga}^d = -\frac{M_a M_w}{M^2} \mathbf{D}_g \mathrm{grad}\left(\frac{p^{ga}}{p^g}\right) = \frac{M_a M_w}{M^2} \mathbf{D}_g \mathrm{grad}\left(\frac{p^{gw}}{p^g}\right) = -\mathbf{v}_{gw}^d, \tag{2.9}$$

because in this case we have

$$\mathrm{grad}\left(\frac{p^{ga}}{p^g}\right) = -\mathrm{grad}\left(\frac{p^{gw}}{p^g}\right). \tag{2.10}$$

In (2.9) $\mathbf{D}_g$ is the effective diffusivity tensor and M is the molar mass of the gas mixture.

2.2. Balance equations

The balance equations are obtained starting from the appropriate local equations expressing the laws of continuum physics (see, for example, Reference 11), specifically the mass balance equation for each species considered, the linear momentum balance equation and the energy balance equation (enthalpy balance) with viscous dissipation and reversible work neglected. In general such equations cannot be

solved at the microscopic level because of the complex geometry of the porous medium, but using spatial averaging techniques,[12-14] the macroscopic balance equations averaged over a representative elementary volume (REV) of the porous medium are obtained. The following balance equations contain already the constitutive equations of the previous section.

The linear momentum balance equation for fluids after neglecting several terms[17-19] gives the generalized Darcy equation

$$\mathbf{v}^{\pi s} = \frac{\mathbf{k} k^{r\pi}}{\mu^{\pi}} [-\text{grad}\, p^{\pi} + \rho^{\pi}(\mathbf{g} - \mathbf{a}^{s} - \mathbf{a}^{\pi s})], \tag{2.11}$$

where $\pi = \text{ga, gw, w, g}$, $\mathbf{v}^{\pi s}$ is the intrinsic mass averaged relative velocity to the solid, $\mathbf{a}^{\pi s}$ is the acceleration relative to the solid and $\mathbf{k} k^{r\pi}/\mu^{\pi}$ expresses the fluid-solid exchange of momentum. The relative permeability $k^{r\pi}$ is a function of the degree of saturation and of temperature, $\mathbf{k}$ is the intrinsic permeability tensor and μ is the dynamic viscosity.

The linear momentum balance equation for the multiphase medium is

$$\text{div}\, \boldsymbol{\sigma} + \rho(\mathbf{g} - \mathbf{a}^{s}) - nS_{w}\rho^{w}\mathbf{a}^{ws} - nS_{g}\rho^{g}\mathbf{a}^{gs} = 0, \tag{2.12}$$

where ρ is the averaged density of the multiphase medium

$$\rho = (1 - n)\rho^{s} + \sum_{\pi \neq s} nS_{\pi}p^{\pi}. \tag{2.13}$$

The dry air mass balance equation, after introduction of Darcy's law and Fick's law and neglecting acceleration terms is

$$\frac{\partial}{\partial t}[nS_{g}\rho^{ga}] + S_{g}\rho^{ga}\text{div}\, \mathbf{v}^{s} - \text{div}\left(\rho^{ga}\frac{\mathbf{k}k^{rg}}{\mu^{g}}\text{grad}\, p^{g}\right) + \text{div}\left(\rho^{g}\frac{M_{a}M_{w}}{M^{2}}\mathbf{D}_{g}\text{grad}\left(\frac{p^{gw}}{p^{g}}\right)\right) = 0. \tag{2.14}$$

The vapour mass balance equation and the water mass balance equation are summed, to obtain the mass balance equation for all water species. Darcy's law and Fick's law are introduced as above, yielding

$$\frac{\partial}{\partial t}[nS_{g}\rho^{gw}] + S_{g}\rho^{gw}\text{div}\, \mathbf{v}^{s} - \text{div}\left(\rho^{gw}\frac{\mathbf{k}k^{rg}}{\mu^{g}}\text{grad}\, p^{g}\right) - \text{div}\left(\rho^{g}\frac{M_{a}M_{w}}{M^{2}}\mathbf{D}_{g}\text{grad}\left(\frac{p^{gw}}{p^{g}}\right)\right) \tag{2.15}$$

$$= -\frac{\partial}{\partial t}(nS_{w}\rho^{w}) + S_{w}\rho^{w}\text{div}\, \mathbf{v}^{s} + \text{div}\left(\rho^{w}\frac{\mathbf{k}k^{rw}}{\mu^{w}}(\text{grad}\, p^{g} - \text{grad}\, p^{c} - \rho^{w}(\mathbf{g} - \mathbf{a}^{s} - \mathbf{a}^{ws}))\right).$$

The macroscopic mass balance equation for the solid has already been summed with the above mass balance equations, to eliminate the time derivative of porosity n. The energy conservation equation (enthalpy balance) is

$$\rho C_{p}\frac{\partial T}{\partial t} - \text{div}\,(\lambda_{\text{eff}}\,\text{grad}\, T)$$
$$- \left[C_{p}^{w}\rho^{w}\frac{\mathbf{k}k^{rw}}{\mu^{w}}(\text{grad}\, p^{g} - \text{grad}\, p^{c} - \rho^{w}(\mathbf{g} - \mathbf{a}^{s} - \mathbf{a}^{ws})) + C_{p}^{g}\rho^{g}\frac{\mathbf{k}k^{rg}}{\mu^{g}}\text{grad}\, p^{g}\right]\text{grad}\, T \tag{2.16}$$

$$= \Delta h_{\text{vap}}\left[\frac{\partial}{\partial t}(nS_{w}\rho^{w}) + S_{w}\rho^{w}\text{div}\, \mathbf{v}^{s} - \text{div}\left(\rho^{w}\frac{\mathbf{k}k^{rw}}{\mu^{w}}(\text{grad}\, p^{g} - \text{grad}\, p^{c} - \rho^{w}(\mathbf{g} - \mathbf{a}^{s} - \mathbf{a}^{ws}))\right)\right],$$

where

$$\rho C_{p} = nS_{w}\rho^{w}C_{p}^{w} + nS_{g}\rho^{g}C_{p}^{g} + (1 - n)\rho^{s}C^{s} \tag{2.17}$$

is the heat capacity of the multiphase medium at constant pressure, λ_{eff} is the effective thermal conductivity and Δh_{vap} the latent heat of evaporation.

2.3. *Initial and boundary conditions*

The initial conditions specify the full fields of gas pressure, capillary or water pressure, temperature and displacements

$$p^g = p_0^g,\ p^c = p_0^c,\ p^w = p_0^w,\ T = T_0,\ \mathbf{u} = \mathbf{u}_0 \quad \text{at } t = t_0. \tag{2.18}$$

The boundary conditions can be imposed values on Γ_π or fluxes on Γ_π^q, where the boundary is $\Gamma=\Gamma_\pi \cup \Gamma_\pi^q$. The imposed values on the boundary for gas pressure, capillary or water pressure, temperature and displacements are as follows:

$$\begin{aligned} &p^g = \hat{p}^g \text{ on } \Gamma_g, \quad p^c = \hat{p}^c \text{ on } \Gamma_c, \quad p^w = \hat{p}^w \text{ on } \Gamma_w, \\ &T = \hat{T} \text{ on } \Gamma_T, \quad \mathbf{u} = \hat{\mathbf{u}} \text{ on } \Gamma_u \quad \text{for } t \geqslant t_0. \end{aligned} \tag{2.19}$$

The volume average flux boundary conditions for water species and dry air conservation equations and the energy equation, to be imposed at the interface between the porous media and the surrounding fluid are the following

$$(\rho^{ga}\mathbf{v}^g - \rho^g\mathbf{v}^{gw})\mathbf{n} = q^{ga} \text{ on } \Gamma_g^q, \tag{2.20a}$$

$$(\rho^{gw}\mathbf{v}^g + \rho^w\mathbf{v}^w + \rho^g\mathbf{v}^{gw})\mathbf{n} = \beta_c(\rho^{gw} - \rho_\infty^{gw}) + q^{gw} + q^w \text{ on } \Gamma_c^q \tag{2.20b}$$

$$-(\rho^w\mathbf{v}^w\Delta h_{vap} - \lambda_{eff}\nabla T)\mathbf{n} = \alpha_c(T - T_\infty) + q^T \text{ on } \Gamma_T^q, \tag{2.20c}$$

where $\mathbf{n}$ is the unit vector, perpendicular to the surface of the porous medium, pointing toward the surrounding gas, ρ_∞^{gw} and T_∞ are, respectively, the mass concentration of water vapour and temperature in the undisturbed gas phase distant from the interface, α_c and β_c are convective heat and mass transfer coefficients, while q^{ga}, q^{gw}, q^w and q^T are the imposed dry air flux, imposed vapour flux, imposed liquid flux and imposed heat flux respectively.

Equations (2.20) are the natural boundary conditions, respectively, for the dry air conservation equation (2.20a), water species conservation equation (2.20b) and energy conservation equation (2.20c), when the solution of these equations is obtained through a weak formulation of the problem, as usually done with the finite element method.

The traction boundary conditions for the displacement field are

$$\boldsymbol{\sigma}\mathbf{n} = \mathbf{t} \text{ on } \Gamma_u^q \quad \text{for } t \geqslant t_0, \tag{2.21}$$

where $\mathbf{t}$ is the imposed traction.

2.4. *Simplified model for cavitation simulation: isothermal monospecies approach*

We consider undrained situations, where cavitation has been experimentally observed. In this situation, with exception of airbubbles in water, which may be observed in fully saturated specimens at low pressures, only two fluid phases are present after cavitation: liquid water and water vapour. An isothermal monospecies approach with two phases is here adopted, where the following balance equations are neglected: the air mass balance equation (2.14) and the energy balance equation (2.16). An isothermal approach means physically that heat can be supplied and taken away with infinite velocity (this implies infinite heat capacity) and that there is no energetic restriction for phase change.

The remaining equations are the linear momentum balance equations (2.11) and (2.12) and the mass

balance equation for water species (2.15). Further we need the perfect gas law for vapour (2.4), Kelvin's equation (2.5), the saturation-capillary pressure relationship (2.1) and the definition of capillary pressure (2.2). Because of the assumption of isothermal behaviour, the Clausius–Clapeyron equation is not needed: p^{gws} in Kelvin's law is then constant and equal to the cavitation pressure.

The following further simplifications are introduced. Because of the absence of dry air flux, the diffusion tensor $\mathbf{D}_g$ is set zero. We neglect the resistance to vapour flux, i.e. $k^{rg}=0$, while the variable relative permeability of water k^{rw} is taken into account (see Figure 1). Also the density of vapour is set to zero in this first approach. These assumptions mean that the left-hand side of (2.15) is equal to zero and that we end up with the balance equation for water in partially saturated regime:

$$0=\frac{\partial}{\partial t}(nS_w\rho^w)+S_w\rho^w\operatorname{div}\mathbf{v}^s+\operatorname{div}\left(\rho^w\frac{\mathbf{k}k^{rw}}{\mu^w}(\operatorname{grad}p^g-\operatorname{grad}p^c-\rho^w(\mathbf{g}-\mathbf{a}^s-\mathbf{a}^{ws}))\right) \tag{2.22}$$

already taken into account in Swandyne code.[9,10] Zero left-hand side means also that vapour flux is neglected, which at low degrees of saturation is justified by the low permeability k^{rg} shown in Figure 1. Because of the assumption of zero density for vapour, (2.4) yields zero vapour pressure. Hence (2.2) reads:

$$p^c=-p^w. \tag{2.23}$$

We have cavitation if absolute pressure of water is equal to the saturated vapour pressure. For instance at 20°C, p^{gws} is equal to 2.889 kPa, while the atmospheric pressure is 101.325 kPa. The relative water pressure at cavitation is equal to $-101.325+2.889=-98.436$ kPa.

Because of the simplifying assumption that vapour pressure is negligible (justified by the above indicated values) we have cavitation at a relative pressure of $-p_{atm}$. Swandyne code works with relative pressures hence from the above assumptions follows that the average pressure, (2.7), in the modified effective stress is:

$$p=S_wp^w. \tag{2.24}$$

This and all the following pressure terms are to be considered relative pressures.

The common employed capillary pressure-saturation relationship is modified accordingly, where a shift of the reference system is necessary, as shown in Figure 2.

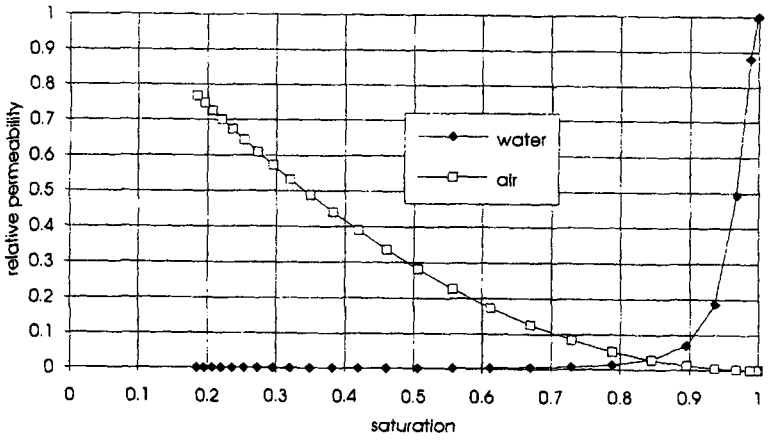

Figure 1. Relative permeabilities for water and gas versus saturation. Values for water taken from Safai and Pinder[21]

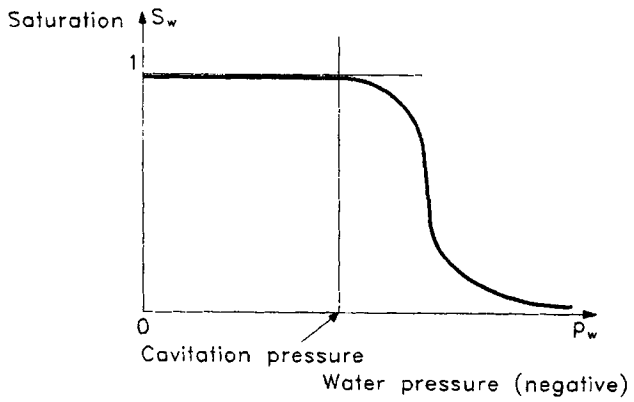

Figure 2. Saturation-water pressure relationship used for modelling cavitation

This rather simple model allows us, however, to take into account the desaturation due to cavitation and the reduced water flux because of the diminishing relative permeability with decreasing degree of saturation. The first example below is solved with this procedure for cavitation.

A more sophisticated approach would require to solve the full equation (2.15) with the fourth term on the left-hand side equal to zero, together with Kelvin's law and the perfect gas law. This possibility is currently investigated. No modification of (2.1) and (2.7) is then needed.

3. DISCRETIZATION AND SOLUTION

With the above simplifications the two remaining balance equations are now the linear momentum balance equation (2.12), where also the relative fluid accelerations are neglected[18] and the mass balance equation (2.22). By ignoring the relative component of the fluid accelerations the primary variables may be reduced to solid displacements and fluid pressure.[18] Further the dynamic seepage forcing term, connected with the solid acceleration is neglected in the mass balance equation because its contribution to the equation system is very small when compared with other terms.[9] The balance equations to be solved, with all the simplified assumptions taken into account, are

$$\operatorname{div} \boldsymbol{\sigma} + \rho(\mathbf{g} - \mathbf{a}^{s}) = \mathbf{0}, \tag{3.1a}$$

$$0 = -\frac{\partial}{\partial t}(nS_w\rho^w) + S_w\rho^w \operatorname{div} \mathbf{v}^s + \operatorname{div}\left(\rho^w \frac{\mathbf{k}k^{rw}}{\mu}(\operatorname{grad} p^g - \rho^w \mathbf{g})\right). \tag{3.1b}$$

Together with the balance equations we need (2.24), the saturation relationships

$$S_w = S_w(p^c), \qquad k^{rw} = k^{rw}(S_w) \tag{3.2}$$

and the appropriate initial and boundary conditions of section 2.3. A weak form of the balance equations is obtained by means of the weighted residual approach as in Reference 10.

The balance equations are then discretized in space using a Galerkin's procedure and in time by Newmark's scheme.[20] The unknown field variables are expressed in the whole domain by global shape function matrices, $\mathbf{N}$ and $\mathbf{N}_w$, and nodal value vectors $\bar{\mathbf{u}}$ and $\bar{\mathbf{p}}^w$

$$\mathbf{u} = \mathbf{N}_u\bar{\mathbf{u}}, \qquad \mathbf{p}_w = \mathbf{N}_w\bar{\mathbf{p}}^w. \tag{3.3}$$

Once the coupling matrix $\mathbf{Q}$, the mass matrix $\mathbf{M}$, the strain operator $\mathbf{B}$ and the external load vector $\mathbf{f}^u$ are introduced (see appendix), the linear momentum balance equation can be written as:

$$\int_\Omega \mathbf{B}^T\sigma' d\Omega - \mathbf{Q}\bar{\mathbf{p}}^w + \mathbf{M}\ddot{\bar{\mathbf{u}}} = \mathbf{f}^u. \tag{3.4}$$

The mass balance equation becomes

$$\mathbf{H}\bar{\mathbf{p}}^{w} + \mathbf{Q}^{T}\dot{\bar{\mathbf{u}}} + \mathbf{S}\dot{\bar{\mathbf{p}}}^{w} = \mathbf{f}^{p}, \tag{3.5}$$

where $\mathbf{H}$ is the permeability matrix, $\mathbf{S}$ the compressibility matrix and $\mathbf{f}^{p}$ the flow vector (see appendix). The coupled system at time t_{n+1} is

$$\begin{aligned} \mathbf{M}_{n+1}\ddot{\bar{\mathbf{u}}}_{n+1} + \bar{\mathbf{P}}_{n+1} - \mathbf{Q}_{n+1}\bar{\mathbf{p}}^{w}_{n+1} &= \mathbf{f}^{u}_{n+1}, \\ \mathbf{Q}^{T}_{n+1}\dot{\bar{\mathbf{u}}}_{n+1} + \mathbf{H}_{n+1}\bar{\mathbf{p}}^{w}_{n+1} + \mathbf{S}_{n+1}\dot{\bar{\mathbf{p}}}^{w}_{n+1} &= \mathbf{f}^{p}_{n+1}, \end{aligned} \tag{3.6}$$

where $\bar{\mathbf{P}}_{n+1}$ is the equivalent nodal force vector. The Newmark scheme adopted for time integration, with the lowest allowable order for each variable, permits to write the variables and their derivatives at t_{n+1} as function of their values at t_n

$$\dot{\bar{\mathbf{u}}}_{n+1} = \dot{\bar{\mathbf{u}}}_{n} + \ddot{\bar{\mathbf{u}}}_{n}\Delta t + \beta_1 \Delta\ddot{\bar{\mathbf{u}}}_{n}\Delta \mathbf{t} = \dot{\bar{\mathbf{u}}}^{p}_{n+1} + \beta_1\Delta\ddot{\bar{\mathbf{u}}}_{n}\Delta \mathbf{t},$$

$$\bar{\mathbf{u}}_{n+1} = \bar{\mathbf{u}}_{n} + \dot{\bar{\mathbf{u}}}_{n}\Delta t + \frac{\ddot{\bar{\mathbf{u}}}_{n}\Delta t^2}{2} + \frac{\beta_2\Delta\ddot{\bar{\mathbf{u}}}_{n}\Delta t^2}{2} = \bar{\mathbf{u}}^{p}_{n+1} + \frac{\beta_2\Delta\ddot{\bar{\mathbf{u}}}_{n}\Delta t^2}{2}, \tag{3.7}$$

$$\dot{\bar{\mathbf{u}}}_{n+1} = \bar{\mathbf{p}}_{n} + \dot{\bar{\mathbf{p}}}_{n}\Delta t + \Theta\Delta\dot{\mathbf{p}}_{n}\Delta t = \dot{\bar{\mathbf{p}}}^{p}_{n+1} + \Theta\Delta\dot{\bar{\mathbf{p}}}_{n}\Delta t,$$

where $\dot{\bar{\mathbf{u}}}^{p}_{n+1}$, $\bar{\mathbf{u}}^{p}_{n+1}$ and $\bar{\mathbf{p}}^{p}_{n+1}$ are predicted values from known parameters at time t_n and β_1, β_2 and Θ are the Newmark's parameters.

Insertion of (3.7) into (3.6) allows the coupled system to be written as:

$$\begin{aligned} \Psi^{u}_{n+1} &= \mathbf{M}_{n+1}\Delta\ddot{\bar{\mathbf{u}}}_{n} + \bar{\mathbf{P}}_{n+1} - \mathbf{Q}_{n+1}\Theta\Delta t\Delta\dot{\bar{\mathbf{p}}}_{n} - \mathbf{F}^{u}_{n+1} = \mathbf{0}, \\ \Psi^{p}_{n+1} &= \mathbf{Q}^{T}_{n+1}\beta_1\Delta t\Delta\ddot{\bar{\mathbf{u}}}_{n} + \mathbf{H}_{n+1}\Theta\Delta t\Delta\dot{\bar{\mathbf{p}}}_{n} + \mathbf{S}_{n+1}\Delta\dot{\bar{\mathbf{p}}}_{n} - \mathbf{F}^{p}_{n+1} = \mathbf{0}. \end{aligned} \tag{3.8}$$

At the beginning of each time step $\bar{\mathbf{P}}_{n+1}$ must be evaluated by integration of the constitutive law, being known the stress field at the previous step.

The non-linear coupled system (3.8) is solved by an iterative procedure. If a Newton–Raphson scheme is adopted to linearize the problem (3.8), i.e.

$$\Psi^{\pi}_{i} + \left.\frac{d\Psi^{\pi}_{i}}{dx}\right|_{x=x_i} dx = 0, \tag{3.9}$$

the Jacobian matrix of transformation, $\mathbf{J}$, at the ith iteration is

$$\mathbf{J} = \left.\frac{\partial\Psi}{\partial x}\right|_{x=x_i} = \begin{pmatrix} \dfrac{\partial\Psi^{u}}{\partial(\Delta\ddot{\bar{\mathbf{u}}})} & \dfrac{\partial\Psi^{u}}{\partial(\Delta\dot{\bar{\mathbf{p}}})} \\ \dfrac{\partial\Psi^{p}}{\partial(\Delta\ddot{\bar{\mathbf{u}}})} & \dfrac{\partial\Psi^{p}}{\partial(\Delta\dot{\bar{\mathbf{p}}})} \end{pmatrix} = \begin{pmatrix} \mathbf{M} + \frac{1}{2}\mathbf{K}_T\beta_2\Delta t^2 & -\mathbf{Q}\Theta\Delta t \\ \mathbf{Q}^{T}\beta_1\Delta t & \mathbf{H}\Theta\Delta t + \mathbf{S} \end{pmatrix}, \tag{3.10}$$

where $\mathbf{K}_T$ is the tangent stiffness matrix.

Substituting (3.10) in (3.9), the system to be solved can then be written in the following form:

$$\begin{pmatrix} \mathbf{M} + \frac{1}{2}\mathbf{K}_T\beta_2\Delta t^2 & -\mathbf{Q}\Theta\Delta t \\ -\mathbf{Q}^{T}\Theta\Delta t & -\dfrac{\Theta}{\beta_1}(\mathbf{H}\Theta\Delta t + \mathbf{S}) \end{pmatrix} \begin{pmatrix} \Delta\ddot{\bar{\mathbf{u}}} \\ \Delta\dot{\bar{\mathbf{p}}} \end{pmatrix} = \begin{pmatrix} -\Psi^{u} \\ -\dfrac{\Theta}{\beta_1}\Psi^{p} \end{pmatrix}. \tag{3.11}$$

It has been made symmetric by a simple scalar multiplication of the second set of equations with the term $-\Theta/\beta_1$. Since the Newton–Raphson method requires the Jacobian matrix to be evaluated and inverted at each iteration, also other modified schemes are used to achieve convergence with less computational effort. In particular, the use of secant updates, like Davidon's and Broyden–Fletcher–Goldfarb–Shanno's (BFGS) methods is found advantageous in non-linear analyses.[9]

4. NUMERICAL RESULTS

As first example we consider the same cross-section as in References 5 and 7 with impervious boundary conditions. Vertical and horizontal displacements are constrained at the bottom surface. Ramp loading is applied at the top, as indicated in Figure 3. The self weight is taken into account as well as hydrostatic pressure distribution as initial condition. The permeability in saturated condition is 0.25×10^{-3} m/s, while once cavitation starts and two phase flow develops, the relationship between degree of saturation and relative permeability of Safai and Pinder[21] has been assumed, see Figure 1. Also the capillary pressure-saturation relationship is that given in Reference 21 but shifted as shown in Figure 2. A Mohr–Coulomb yield criterion with softening is used within the framework of associative plasticity and the material parameters are the following: Young's modulus, $E = 285$ MPa; Poisson's ratio, $\nu = 0.4285$; solid grain density, $\rho^s = 2000$ kg/m^3; liquid density, $\rho^w = 1000$ mg/m^3; apparent cohesion, $c_0 = 1.84$ MPa; hardening modulus, $H = -40$ MPa; angle of internal friction, $\varphi = 20°$; initial porosity, $n = 0.20$; solid grain bulk modulus, $K_s = 6.78$ GPa; liquid phase bulk modulus, $K_w = 0.20$ GPa.

Shear band formation starts from the bottom surface when the first crest of loading wave hits the boundary. The development of the shear band is shown in Figures 4, 5 and 6, where the equivalent plastic strain contours at 0.18, 0.215 and 0.235 s are respectively depicted. The pore water traction (which means capillary pressure, equation (2.23)) distribution at 0.235 s is shown in Figure 7 (the code used for these simulation assumes pore pressure positive in traction). The flow rate with and without modelling cavitation are shown in Figure 8 and 9 respectively. It should be noted that without

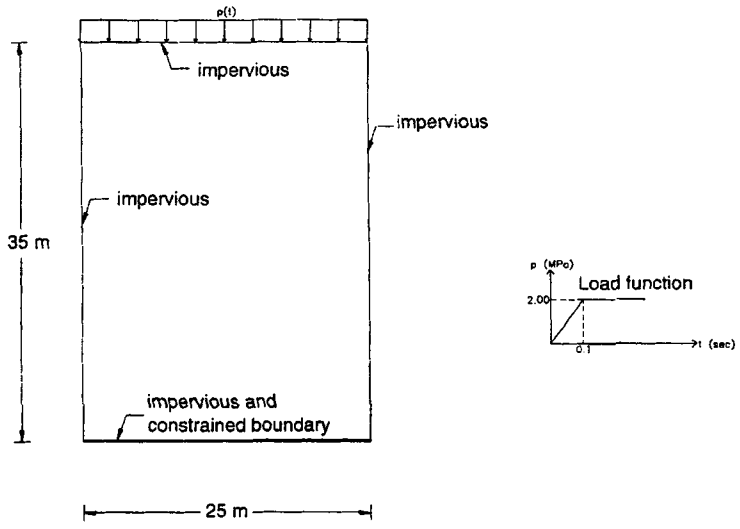

Figure 3. Geometrical characteristics and load function of the first example

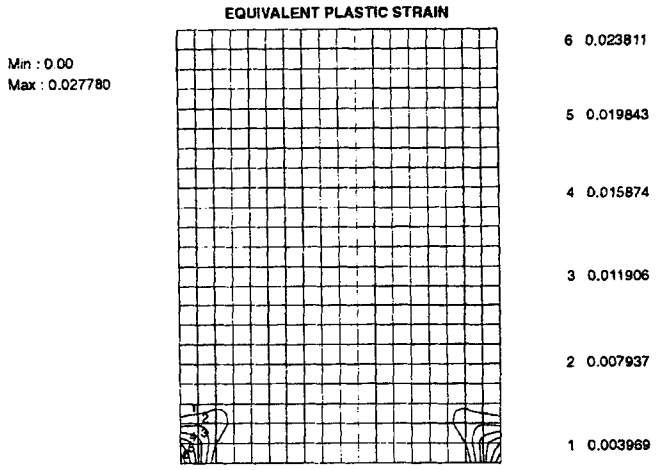

Figure 4. Effective plastic strain at $t = 0.18$ s

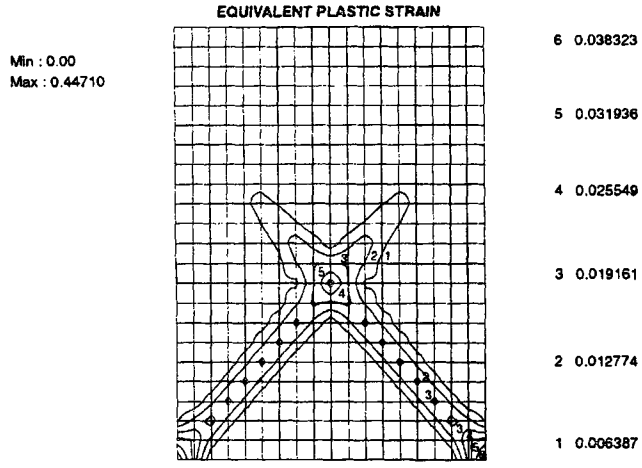

Figure 5. Effective plastic strain at $t = 0.215$ s

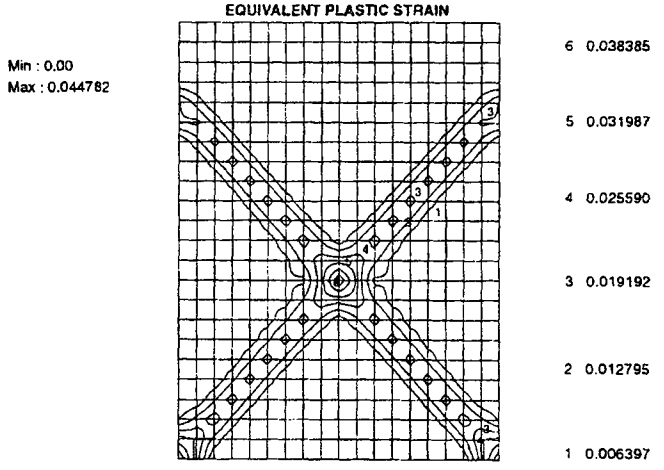

Figure 6. Effective plastic strain at $t = 0.235$ s

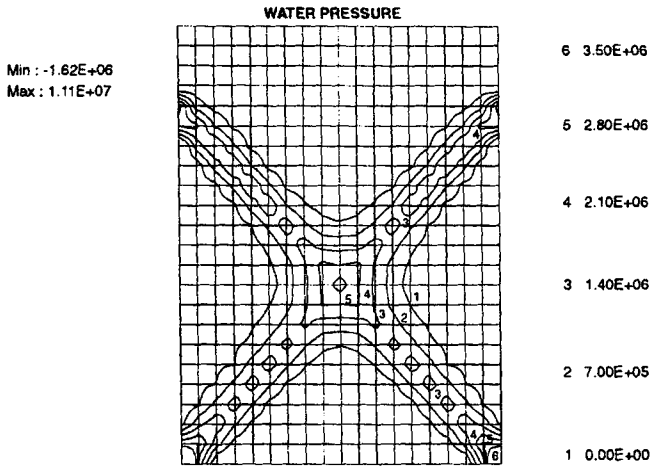

Figure 7. Pore water tractions (Pa) at 0.235 s

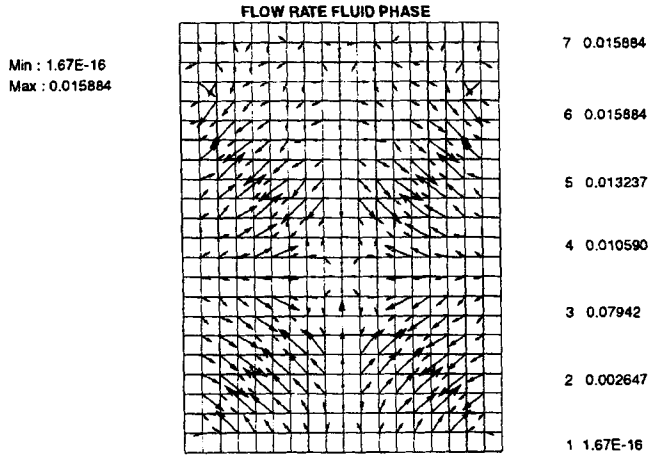

Figure 8. Flow rate of fluid phase at $t = 0.235$ s with cavitation modelling

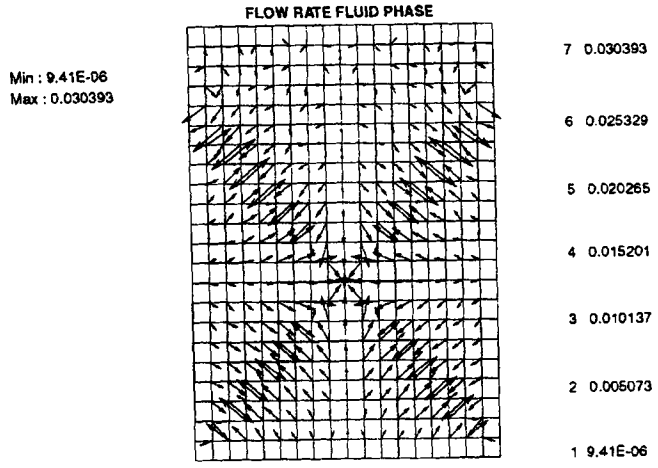

Figure 9. Flow rate of fluid phase at $t = 0.235$ s without modelling cavitation

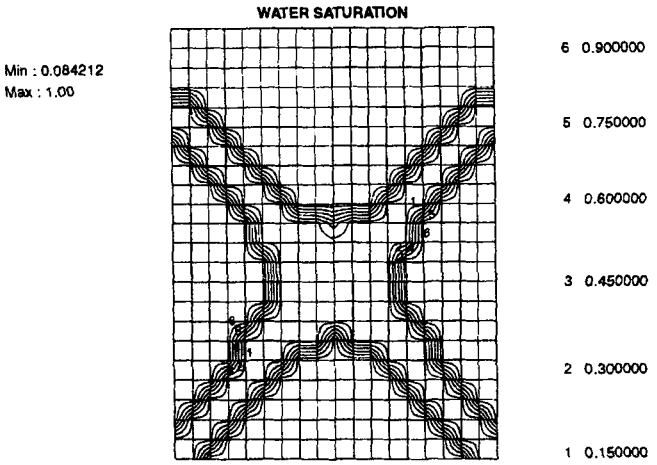

Figure 10. Distribution of degree of water saturation at $t = 0.235$ s

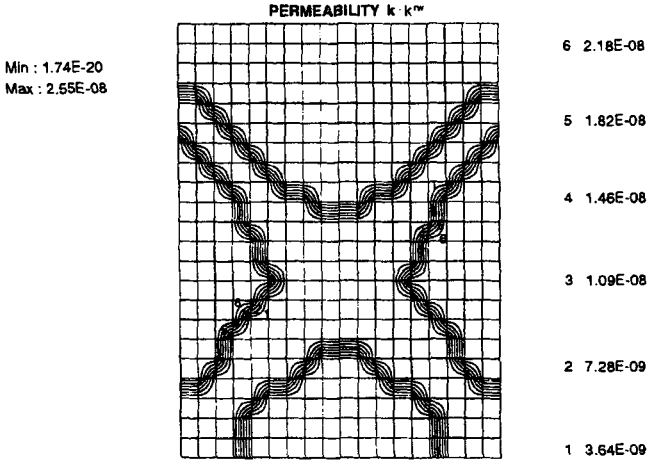

Figure 11. Distribution of absolute permeability at $t = 0.235$ s

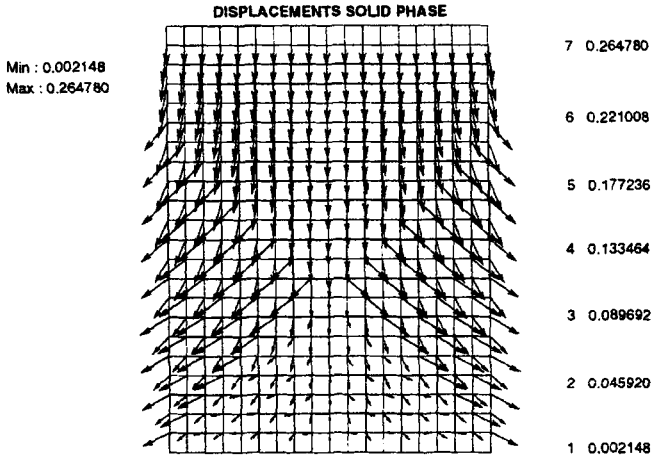

Figure 12. Displacement vectors at $t = 0.235$ s

cavitation the flow rate is approximately doubled. The distribution of the degree of saturation can be seen in Figure 10 and the permeability $\mathbf{k}k^{rw}$ distribution is drawn in Figure 11. The displacement of the solid phase after the full development of the shear band is depicted in Figure 12. Pore water pressure, which is to be considered capillary pressure in the traction range, and vertical total strain versus time at a nodal point and at a gauss point inside and outside the shear band (at the same level below the centre) can be seen in Figures 13 and 14.

The weak mesh dependence of the maximum effective plastic strain is shown on a second example. The case studied in Reference 7 has been used for this purpose. The same cross-section as above is investigated but with lateral surfaces open to flow. The sample is further subject to axial compression by means of uniform ramp loading both on the upper and lower surfaces. Initial stress state and initial pressure are zero. The material parameters as the same as above, with apparent cohesion $c_0 = 1.42$ Mpa instead of 1.84 MPa. Meshes made of 18 × 22 (396 f.e.), 24 × 30 (720 f.e.), 30 × 36 (1080 f.e.) and 36 × 44 (1584 f.e.) rectangular four node elements where used. For the mesh of 396 elements in Figures 15 and 16 the equivalent plastic strain contours at 0.35 and 0.50 s are shown respectively. Shear band formation starts from the centre of the sample (Figure 15) because of the loading condition chosen. Pore water traction at 0.50 s is shown in Figure 17.

The resulting effective plastic strains after full development of the shear band along two vertical cross-sections at the centre and at the quarter of the model are drawn in Figures 18 and 19. Without regularization these maxima would severely change for the four meshes considered (compare e.g. for a single phase material Reference 22). These figures confirm hence that a diffusion (flow) governed model contains a natural regularization procedure.

We are currently investigating the model parameters which control this regularization and the associated internal length scale.

This second example, which has been solved without considering phase change, shows that at least numerically, cavitation is not strictly necessary for the shear band to develop. In this case the shear band develops from the centre when significant pore water tractions appear.[7]

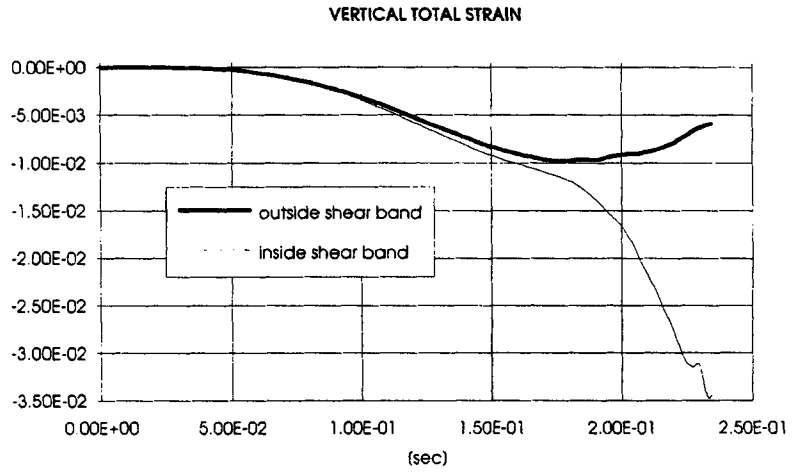

Figure 13. Total vertical strains at two gauss points slightly below the centre, one inside, the other outside the shear band

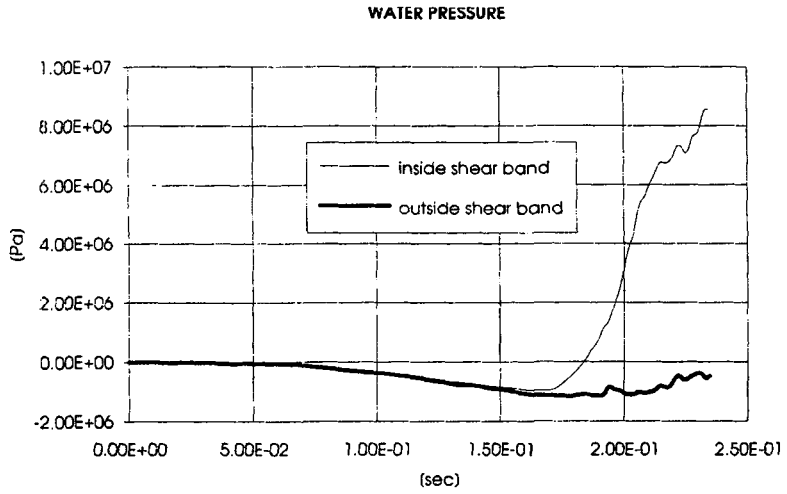

Figure 14. Water pressure at two nodals points slightly below the centre, one inside, the other outside the shear band

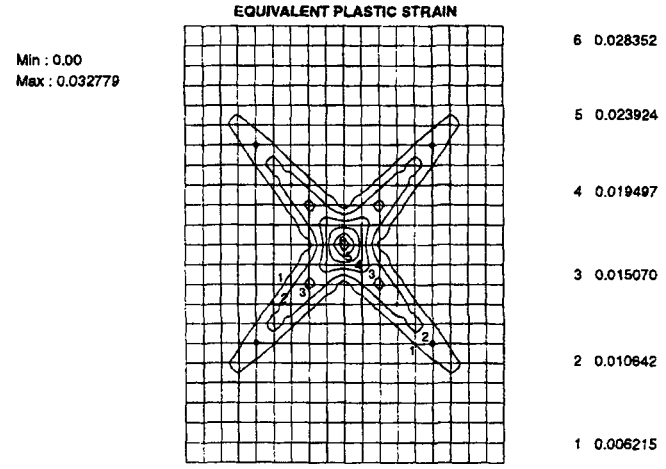

Figure 15. Effective plastic strain at $t = 0.35$ s

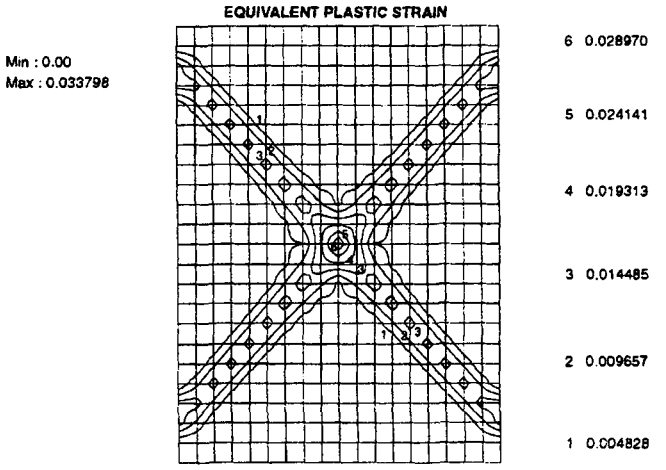

Figure 16. Effective plastic strain at $t = 0.50$ s

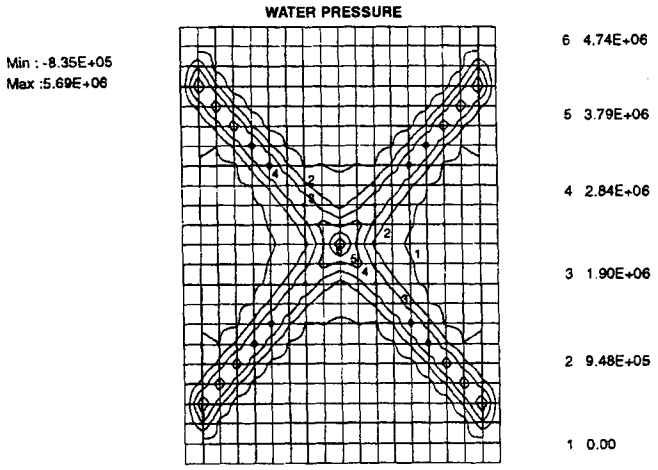

Figure 17. Pore water tractions (Pa) at 0.50 s

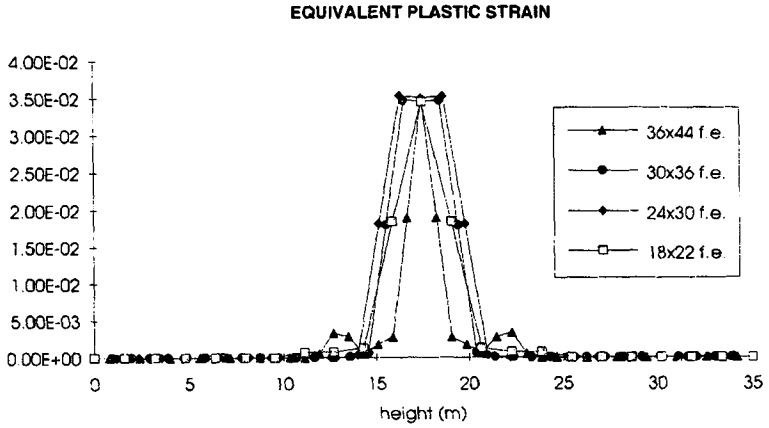

Figure 18. Equivalent plastic strain for different meshes along a vertical cross section through the centre

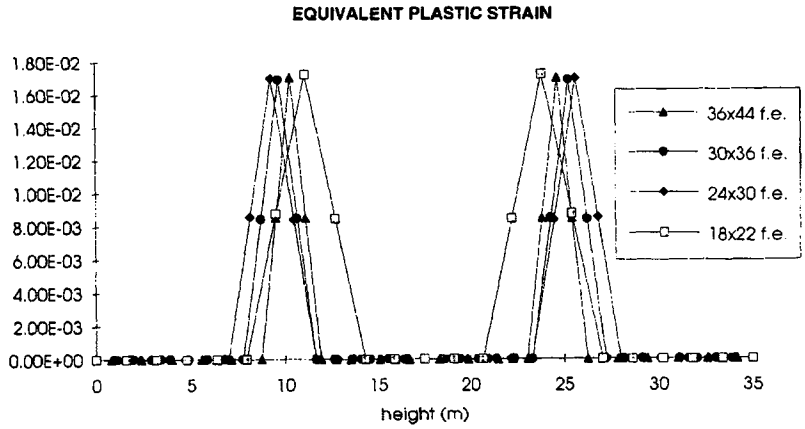

Figure 19. Equivalent plastic strain for different meshes along a vertical cross section at a quarter of the base

4.1. Shear band inclination

Shear band inclination in a single phase material depends on many parameters such as friction angle, dilatancy angle, Poisson's ratio and hardening modulus.[23] In a multiphase material the influence of the liquid phase is fundamental: shear band inclination depends also on permeability values and on the boundary conditions of fluid phase.

In classical plasticity, Mohr–Coulomb theory and von Mises theory give two typical values for the shear band inclination.

In drained conditions, the influence of volumetric strain is important; Mohr–Coulomb theory states that the shear band is parallel to the surface which is subject to the stress (σ, τ) of the Mohr–Coulomb failure envelope. The shear band makes hence the following angle θ with the major principal stress direction

$$\theta = \tfrac{1}{4}\pi - \tfrac{1}{2}\phi,$$

where ϕ is the friction angle. Using $\phi = 20°$, this theory gives $\theta = 35°$. This theory does not take into account fluid phase as done in the numerical model. With a permeability value of 25 m/s (unrealistic value which should simulate drained conditions restricting water contribution), in Figure 20 an inclination angle of $\theta = 38°$ is shown. In this case the boundary conditions adopted are: impermeable top and bottom surface, lateral surface open to flow.

In perfectly undrained conditions, von Mises yield criterion may be used to obtain a reference value because no volumetric strains appear[24]. This criterion states that inclination angle in plane strain case is[22]

$$\theta = \frac{(1-\nu)s_1 - \nu s_2}{\nu s_1 - (1-\nu)s_2},$$

where s_1 and s_2 are the principal deviatoric stresses.

Using a Poisson's ratio $\nu = 0.4285$, this equation gives $\theta = 45.8°$. A numerical experiment with plane strain elements and von Mises yield criterion gave this theoretical value. In Figure 6 an inclination angle of 42° can be seen; in that case there is internal flow and a Mohr–Coulomb law has been used hence the above limit does not apply exactly.

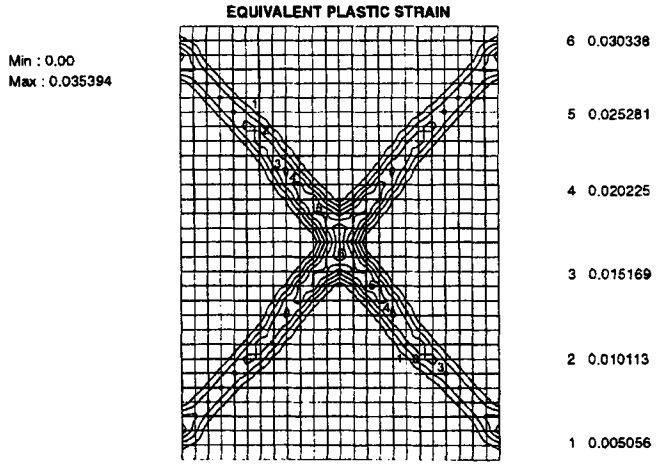

Figure 20. Effective plastic strain at $t = 0.36$ s

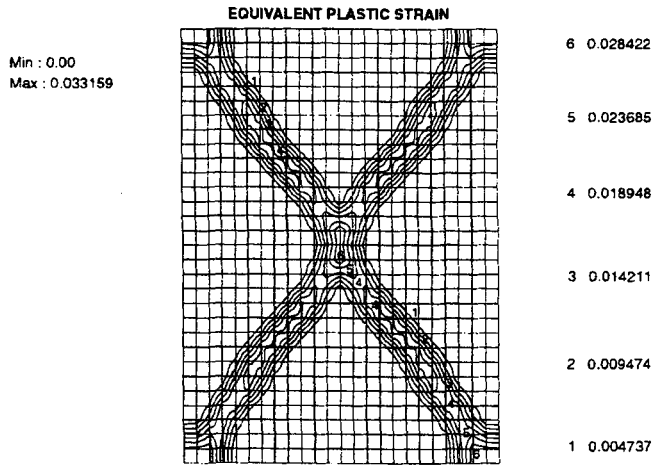

Figure 21. Effective plastic strain at $t = 0.22$ s

It is also observed that with four node elements it is not easy to capture the correct value of shear band inclination, especially using a large element, as shown in Figure 16, where a drained sample with lateral surfaces open to flow is analysed and a value of $\theta = 42°$ is observed.

The influence of fluid boundary conditions on shear band inclination can be seen from the following numerical test. In a first sample upper and bottom surfaces are open to flow, while lateral surfaces are impervious. With a permeability value of 0.25 m/s, inclination angle $\theta = 36°$ is obtained as shown in Figure 21. Using impervious upper and bottom surfaces and lateral surfaces open to flow, an inclination angle of $\theta = 41.5°$ is obtained.[7]

CONCLUSION

It has been shown that not only experimentally but also numerically negative pore pressures may be obtained in localisation phenomena in fully saturated undrained samples of dilatant geomaterials. In the numerically investigated case a Mohr–Coulomb constitutive relationship with a softening branch has been used within the framework of associative plasticity.

The rapidly decreasing pore pressure in the process of shear band formation reaches the point where cavitation is of importance. A facility to model this situation based on simplified balance equations has been developed and implemented in the code Swandyne for partially saturated soil dynamics. This allows to follow more closely the phenomena which take place after the onset of the instability, as shown in an example.

The model, being diffusion (flow) governed, contains further a natural regularization procedure which allows to obtain shear bands with substantially mesh size independent maximum effective plastic strain. This has been demonstrated on a further example.

ACKNOWLEDGEMENTS

This work has been carried out within the framework of HCM project 'ALERT geomaterials' and was partly financed by the Italian Ministry of Scientific and Technological Research (MURST 40%).

APPENDIX

coupling matrix

$$\mathbf{Q} = \int_\Omega \mathbf{B}^{\mathrm{T}} S_{\mathrm{w}} \mathbf{m} \mathbf{N}_{\mathrm{w}} \mathrm{d}\Omega \qquad \text{with } \mathbf{m} = (1, 1, 1, 0, 0, 0)^{\mathrm{T}}$$

mass matrix

$$\mathbf{M} = \int_\Omega \mathbf{N}_u^T [\rho^{\mathrm{s}}(1-n) + \rho^{\mathrm{w}} n S_{\mathrm{w}}] \mathbf{N}_{\mathrm{u}} \mathrm{d}\Omega$$

permeability matrix

$$\mathbf{H} = \int_\Omega (\nabla \mathbf{N}_w)^{\mathrm{T}} \mathbf{k} \nabla \mathbf{N}_{\mathrm{w}} \mathrm{d}\Omega$$

compressibility matrix

$$\mathbf{S} = \int_\Omega \mathbf{N}_w^T \frac{1}{Q} \mathbf{N}_{\mathrm{w}} \mathrm{d}\Omega$$

external load vector

$$\mathbf{f}^{\mathrm{u}} = \int_\Omega \mathbf{N}_u^T [\rho^{\mathrm{s}}(1-n) + \rho^{\mathrm{w}} n S_{\mathrm{w}}] \mathbf{g} \mathrm{d}\Omega + \int_\Gamma \mathbf{N}_u^T \mathbf{t} \mathrm{d}\Gamma$$

flow vector

$$\mathbf{f}^{\mathrm{p}} = \int_\Omega (\nabla \mathbf{N}_{\mathrm{w}})^{\mathrm{T}} \mathbf{k} \rho^{\mathrm{w}} \mathbf{g} \mathrm{d}\Omega - \int_{\Gamma_{\mathrm{w}}} \mathbf{N}_p^T \mathbf{q}^{\mathrm{T}} \mathbf{n} \mathrm{d}\Gamma$$

equivalent force vector

$$\bar{\mathbf{P}} = \int_\Omega \mathbf{B}^{\mathrm{T}} \sigma' \mathrm{d}\Omega$$

$$\mathbf{F}_{n+1}^{\mathrm{u}} = \mathbf{f}_{n+1}^{\mathrm{u}} - \mathbf{M}_{n+1} \ddot{\mathbf{u}}_n + \mathbf{Q}_{n+1} (\bar{\mathbf{p}}_n + \Delta t \dot{\bar{\mathbf{p}}}_n)$$

$$\mathbf{F}_{n+1}^{\mathrm{p}} = \mathbf{f}_{n+1}^{\mathrm{p}} - \mathbf{Q}_{n+1}^{\mathrm{T}} (\dot{\mathbf{u}}_n + \Delta t \ddot{\mathbf{u}}_n) - \mathbf{H}_{n+1} (\bar{\mathbf{p}}_n + \Delta t \Delta \dot{\mathbf{p}}_n) - \mathbf{S}_{n+1} \dot{\bar{\mathbf{p}}}_n$$

$$\frac{1}{Q} = C_{\mathrm{ww}} + \frac{C_{\mathrm{wg}}}{S_{\mathrm{g}}} \frac{C_{\mathrm{s}}}{n} p^{\mathrm{w}} + C_{\mathrm{s}} = C_{\mathrm{s}} + \frac{n S_{\mathrm{w}}}{K_{\mathrm{w}}} + \frac{(\bar{\alpha} - n)}{K_{\mathrm{s}}} S_{\mathrm{w}} \left(S_{\mathrm{w}} + \frac{C_{\mathrm{s}}}{n} p^{\mathrm{w}} \right)$$

$$C_{\mathrm{ww}} = \frac{(\bar{\alpha} - n)}{K_{\mathrm{s}}} S_{\mathrm{w}}^2 + \frac{n S_{\mathrm{w}}}{K_{\mathrm{w}}}$$

$$C_{\mathrm{wg}} = \frac{(\bar{\alpha} - n)}{K_{\mathrm{s}}} S_{\mathrm{w}} (1 - S_{\mathrm{w}})$$

$$C_{\mathrm{gg}} = \frac{(\bar{\alpha} - n)}{K_{\mathrm{s}}} (1 - S_{\mathrm{w}})^2 + \frac{n(1 - S_{\mathrm{w}})}{K_{\mathrm{g}}}$$

$$C_{\mathrm{s}} = n \frac{\mathrm{d}S_{\mathrm{w}}}{\mathrm{d}p^{\mathrm{w}}}$$

NOTATION

s	solid phase
g	gaseous phase
w	liquid phase
π	generic phase
$\mathbf{a}^{\pi}$	acceleration of π phase
$\mathbf{a}^{\pi s}$	acceleration relative to the solid
$\mathbf{B}$	strain operator
C_s	specific capacity
$\mathbf{C}_T$	tangential constitutive tensor
$\mathbf{D}_g$	effective diffusivity tensor
$\mathbf{f}^p$	flow vector
$\mathbf{f}^u$	external load vector
$\mathbf{g}$	gravity acceleration
$\mathbf{H}$	permeability matrix
$\mathbf{I}$	unit tensor
$k^{r\pi}$	liquid phase relative permeability
$\mathbf{k}$	absolute or intrinsic permeability tensor
$k = \mathbf{k}k^{r\pi}\rho^w g/\mu$	permeability value [L/t]
K_s	solid grain bulk modulus
K_w	liquid phase bulk modulus
$\mathbf{K}_T$	tangential stiffness tensor
M_π	molar mass of constituent π
$\mathbf{M}$	mass matrix
n	porosity
$\mathbf{n}$	unit normal vector
p^{π}	macroscopic pressure of the π phase
$\bar{\mathbf{P}}$	equivalent force vector
$\mathbf{Q}$	coupling matrix
R	universal gas constant
S_w	water saturation
S_g	gas saturation
$\mathbf{S}$	compressibility matrix
t	time variable
$\mathbf{t}$	surface traction tensor
T	temperature
$\mathbf{u}$	solid displacements
$\mathbf{v}^{\alpha\pi}$	velocity of the α-phase with respect to the π phase
$\mathbf{v}^{\pi}$	velocity of the π phase
$\bar{\alpha}$	Biot's coefficient
β_1, β_2, Θ	Newmark's parameters
λ_{eff}	effective thermal conductivity
μ	liquid dynamic viscosity
ρ	porous medium density
ρ^{π}	intrinsic phase averaged density of the π phase
$\boldsymbol{\sigma}$	Cauchy stress tensor
$\boldsymbol{\sigma}'$	effective stress tensor

Variables with overbar refer to the nodal values.

REFERENCES

1. O. Reynolds, 'On the dilatancy of media composed of rigid particles in contact, with experimental illustrations', *Philos, Mag.*, **20**, 469–481 (1885). (Reprinted in O. Reynolds *Papers on Mechanical and Physical Subjects*, vol. 2, Cambridge University Press, New York, pp. 203–216, 1901.)
2. J. R. Rice, 'On the stability of dilatant hardening for saturated rock masses', *J. Geophys. Res.*, **80**, 1531–1536 (1985).
3. J. W Rudnicki, 'Effect of dilatant hardening on the development of concentrated shear-deformation in fissured rock masses', *J. Geophys. Res.*, **89** 9259–9270 (1984).
4. I. Vardoulakis, 'Dynamic stability analysis of undrained simple shear on water-saturated granular soils', *Int. J. Numer. Anal. Meth. Geomech.*, **10**, 177–190, (1986).
5. B. Loret and J.H. Prevost, 'Dynamic strain localisation in fluid-saturated porous media' *J. Eng. Mech.*, **11**, 907–922, (1991).
6. M. Mokni, Relations entre déformations en masse et déformations localisées dans les matériaux granulaires, Ph. D. Thesis, Institut de Mécanique de Grenoble, France, 1992
7. B.A. Schrefler, C.E. Majorana and L. Sanavia, 'Shear band localization in saturated porous media', *Arch. of Mech.*, **47**, 577–599 (1995).
8. D. Gawin, P. Baggio and B. A. Schrefler, 'Coupled heat, water and gas flow in deformable porous media', *Int. J. Numer. Meth. Fluids*, **20**, 969–987, (1995).
9. Y. M. Xie, Finite element solution and adaptive analysis for static and dynamic problems of saturated-unsaturated porous media, Ph.D. Thesis, C/Ph/136/90, Department of Civil Engineering, Swansea University, Great Britain, 1990
10. E.A. Meroi, B.A. Schrefler and O.C. Zienkiewicz, 'Large strain static and dynamic semisaturated soil behaviour', *Int. J. Num. Anal. Meth. Geomech.*, **19**, 81–106, (1995).
11. B. A. Schrefler, 'F.E. in environmental engineering: coupled thermo-hydro-mechanical processes in porous media including pollutant transport', *Arch. Comput. Meth. Eng.*, **2**, 1–54, (1995).
12. M. Hassanizadeh and W. G. Gray, 'General conservation equations for multi-phase system: 1. Averaging technique', *Adv. Water Res.*, **2**, 131–144, (1979).
13. M. Hassanizadeh and W. G. Gray, 'General conservation equations for multi-phase system: 2. Mass, momenta, energy and entropy equations', *Adv. Water Res.*, **2**, 191–201, (1979).
14. M. Hassanizadeh and W.G. Gray, 'General conservation equations for multi-phase system: 3. Constitutive theory for porous media flow', *Adv. Water Res.*, **3**, 25–40, (1980).
15. W. G. Gray and M. Hassanizadeh, 'Unsaturated flow theory including interfacial phenomena', *Water Resources Res.*, **27**, 1855–1863, (1991).
16. ASHRAE Handbook, *Fundamentals Volume*, ASHRAE, Atlanta, 1993.
17. R. W. Lewis and B. A. Schrefler, *The finite element method in the static and dynamic deformation and consolidation of porous media*, John Wiley, New York, 1996.
18. O. C. Zienkiewicz, A. H. C. Chan., M. Pastor, D. K. Paul and T. Shiomi, 'Static and dynamic behaviour of soils: a rational approach to quantitative solutions. I. Fully saturated problems', *Proc. R. Soc. Lond.* A **429**, 285–309 (1990).
19. O. C. Zienkiewicz, Y. M. Xie, B. A. Schrefler, A. Ledesma and N. Bicanic, 'Static and dynamic behaviour of soils: a rational approach to quantitative solutions. II. Semi-saturated problems', *Proc. R. Soc. Lond.* A **429**, 311–321, (1990).
20. O. C. Zienkiewicz and R. L. Taylor, The finite element method, vol. 2, McGraw-Hill Book Company, London, 1991.
21. N. M. Safai and G. F. Pider, 'Vertical and horizontal land deformation in a desaturating porous medium', *Adv. Water Resour.*, **2**, 19–25, (1979).
22. L. J. Sluys, Wave propagation, localisation and dispersion in softening solids, PhD Thesis, Technische Universiteit Delft, Netherlands, 1992.
23. J. P. Bardet, 'A comprehensive review of strain localization in elastoplastic soils', *Computers and Geotechnics*, **10**, 163–188, (1990).
24. H. Maosong, New developments in numerical analysis of dynamic and static soil problems, Ph.D. Thesis, C/Ph/185/95, Department of Civil Engineering, Swansea University, Great Britain, 1995.